Changes of the Commensal Microbiome during Treatment are Associated with Clinical Response in Nasopharyngeal Carcinoma Patients

Tingting Huang[a, b, c], Justine Debelius[a], Alexander Ploner[a], Xiling Xiao[d], Tingting Zhang[b, c], Kai Hu[b, c], Zhe Zhang[d], Rensheng Wang[b, c, #], Weimin Ye[a, #]

[a] Department of Medical Epidemiology and Biostatistics, Karolinska Institutet, Stockholm, Sweden

[b] Department of Radiation Oncology, The First Affiliated Hospital of Guangxi Medical University, Nanning, P. R. China

[c] Radiation Oncology Clinical Medical Research Center of Guangxi, Nanning, Nanning, P. R. China

[d] Department of Otolaryngology-Head & Neck Surgery, First Affiliated Hospital of Guangxi Medical University, Nanning, P. R. China.

Running title: Microbiome is Associated with Clinical Response in NPC

Address correspondence to Weimin Ye (weimin.ye@ki.se) and Rensheng Wang (wangrenshenggxmu@gmail.com).

Weimin Ye and Rensheng Wang contributed equally to this work. Author order was determined by consortium policy.

Abstracts

The human microbiome has been suggested to be involved in the regulation of response to anticancer therapies. However, little is known regarding changes of commensal microbes in cancer patients during radiotherapy and whether these changes are associated with response to treatment. We conducted a prospective, longitudinal cohort with sixty-two newly diagnosed nasopharyngeal carcinoma (NPC) patients who were scheduled for radiotherapy-based treatment. Nasopharyngeal swabs were collected longitudinally before radiotherapy, during radiotherapy, and after radiotherapy. The nasopharyngeal microbiome was assessed using 16S rRNA amplicon sequencing. All patients were followed up to 24 months to define an early or late clinical response. We demonstrated the beta-diversity of the nasopharyngeal microbiome showed temporal changes throughout treatment. The magnitude of changes was stably and significantly different between the early and late responders. The temporal microbial networks among NPC patients with early response differed significantly from those with late response. Seven amplicon sequence variants (ASVs) mapped to *Corynebacterium* were lost during treatment. Twenty-eight abundant ASVs differed by patients' responses throughout treatment. Among them, 10 ASVs differed between the early responders and late responders before getting any treatment and the difference was consistent along the radiotherapy course. This study addressed the temporal changes of the nasopharyngeal microbiome in NPC patients during radiotherapy and suggested a significant association with clinical response. The subject-specific changes of the nasopharyngeal microbiome might serve as a potential predictor for clinical response to radiotherapy.

Importance

The human microbiome has been suggested to be involved in the regulation of response to anticancer therapies. However, little is known regarding changes of commensal microbes in cancer patients during radiotherapy and whether these changes have an impact on response to treatment. In this longitudinal study of nasopharyngeal carcinoma patients, we demonstrate that the temporal changes of the nasopharyngeal microbiome in NPC patients during radiotherapy-based treatment and suggest a significant association with patients' clinical response. We identify 28 abundant amplicon sequence variants differed significantly between the early and late responders throughout treatment. Among them, 10 are consistently differed by patients' responses. These subject-specific changes might serve as a potential predictor for clinical response to radiotherapy. To the best of our knowledge, this is the first example that the commensal microbiome may influence the response to radiotherapy-based treatment in cancer patients.

Introduction

The human commensal microbiome has been suggested to be involved in both carcinogenesis and in the regulation of response to anticancer therapies (1-4). Accumulating evidence suggests that the microbiome can substantially affect the effectiveness of chemotherapy and immunotherapy such as gemcitabine and immune checkpoint inhibitors (5, 6). Accordingly, there is a growing interest in identifying and targeting these microbes in the anti-cancer treatment. However, little is known regarding whether or how the microbiome may regulate the response to radiotherapy, which is critical to the realization of its potential (2, 3, 7). In part, this is due to a lack of well designed longitudinal studies looking at the relationship between microbes and response to radiotherapy is seldom studied (2, 3).

To address this knowledge gap, we conducted a prospective study to characterize the longitudinal patterns of the commensal microbiome among cancer patients during radiotherapy-based anti-cancer treatment and investigated whether the temporal changes of the microbiome might be associated with patients' clinical response. Nasopharyngeal carcinoma (NPC) is a malignant disease and endemic mainly in southern China and Southeast Asia (8). Radiotherapy is the essential mainstay of curative-intent treatment for the non-disseminated disease. Intensity-modulated radiation therapy (IMRT) contributes to the high 5-year survival rate of 68-80%, together with chemotherapy (9, 10). However, both local and distant failure after a first-line therapy remain key challenges which call for identification of novel indicators and modulators of clinical response. Hence, we prospectively collected nasopharyngeal swab samples during radiotherapy from a hospital-based NPC-patient cohort in southern China where NPC incidence rates exceed 10-15 per 100 000 person-years, about twenty times the rate in the western world (8). We hypothesized that the temporal change of

nasopharyngeal microbiome during radiotherapy might be associated with NPC patients' clinical responses.

Results

A total of 445 nasopharyngeal microbial profiles, corresponding to 39 NPC patients, were analyzed. Thirty-six (92.3%) patients had advanced disease (stage III to IV_B) at diagnosis. All of the NPC patients were treated with radiotherapy, 35 (89.7%) received concurrent chemotherapy including 25 (64.1%) who received induction chemotherapy or adjuvant chemotherapy. Twenty-seven patients (69.2%) with CR at the first clinical check-up were defined as early responders; the remaining 12 NPC patients achieved CR within 24 months of follow-up were defined as late responders (Supplementary Table S1).

NPC patients' clinical responses are associated with the temporal changes of between-sample diversity of nasopharyngeal microbiome during radiotherapy

The overall pattern of beta-diversity of the nasopharyngeal microbiome was visualized in PCoA projections for both unweighted and weighted UniFrac distance (Supplementary Figure S1). In both PCoA projections, samples of early responders were relatively dissimilar with the samples of late responders along PC2 (explained 5.88% of the variation in the unweighted projection; and 12.93% of the variation in the weighted projection), while similar along PC1 (13.23% in the unweighted, and 29.50% in the weighted) and PC3 (3.59% in the unweighted, and 7.84% in the weighted). By performing volatility analysis, the global variation (as an average) along PCs as a measure of longitudinal temporal volatility is presented in Figure 1. We saw a consistent shift along with the PC1 space with sampling time in both unweighted

and weighted panels, regardless of clinical response. In PC2 panels, distinct separations between early and late responders were observed throughout treatment, whereas the temporal trajectories were relatively stable in each group. Moreover, in PC3 space, a moderate separation between the trajectories of response groups was found in the unweighted panel while the trajectories in the weighted panel showed fluctuated and gradual directional changes throughout treatment regardless of response status. The changed volatilities found in the last few sampling time-points have a larger standard deviation compared to the previous time-points, which might be partially explained by low sample numbers. Patient compliance with sample collection varied.

We measured the rate of change in beta-diversity differences over radiotherapy in terms of the weighted UniFrac step length Δ-wUF and tested whether Δ-wUF changed over treatment and in response to the response status of NPC patients. We found statistically significant evidence for subject-specific differences (random effects) in baseline step length (intercept) as well as a change in step length over sampling time (slope, *P*-value = 0.0005) from linear mixed effect models (Supplementary Table S2). However, the across-subject average step length (fixed effect) appeared stable in Figure 2A, with no evidence for increasing or decreasing dynamic change (*P*-value = 0.4609). Adding the clinical response status improved the mixed effect model significantly (*P*-value = 0.0152). The best-fitting model including clinical response status retained stable for average step lengths for both early and late responders, with larger average step lengths for early responders compared to late responders (Figure 2B). Individual trajectories varied considerably between subjects, shown in Figure 2C.

NPC patients' clinical responses are associated with the temporal trajectories of the abundant microbial features

Seventy-three ASVs were identified as the abundant subset for feature-based analyses. A Procrustean randomization test and Mantel test based on the Bray-Curtis distance indicated a well concordance between the abundant subset and the full dataset (PROTEST: correlation = 0.9669, *P*-value = 0.001, 999 permutations; Mantel test: correlation = 0.9506, *P*-value = 0.001, 999 permutations; Supplementary Figure S2). NMIT evaluates interdependence networks, which summarized the temporal trajectories of the abundant subset over treatment of each NPC patient into a single distance. The NMIT distances differed between clinical response groups. We observed that the interdependence networks among patients with early response statistically significantly differed from those with a late response, and no statistically significance differences found within response groups (PERMANOVA: *P*-value = 0.014; permdisp: *P*-value = 0.315; 999 permutations). In Figure 3, the networks of the late responders varied widely, forming a spread ellipsoid-like cluster, compared to the early responders who formed a smaller and more constrained ellipsoid-like cluster. These clusters are dissimilar along PC1 and PC3, but relatively similar along PC2.

We investigated longitudinal changes in the abundant ASVs across all samples using a modified ANCOM-test. We identified seven abundant ASVs where more than 80% of ASV ratios were temporally correlated (Supplementary Figure S3, panel A), all members of genus *Corynebacterium*. There was a decrease in the relative abundance of all seven ASVs showed during treatment while most other ASVs remained stable over treatment course (Supplementary Table S3; and Figure S3, panel B to E).

To quantify ASV-based longitudinal differences between early and late responders, we applied SS-ANOVA. We identified 28 out of 73 abundant ASVs as differing significantly between early and late responders over treatment course, listed in Table 1 (*P*-value < 0.05, 1500 permutations). Notable that, among these significant ASVs, 10 differed between the early responders and late responders before getting any treatment, and remained consistently different during radiotherapy. Additionally, there were 9 ASVs that were similar between response groups during the first one-third of treatment and became different until the completion. In contrast, 5 ASVs differed between groups at the beginning and was converged during treatment.

For better visualization of the temporal trajectories of the difference between the early and late responders, the log2-fold changes of the 73 abundant ASVs estimated by SS-ANOVA were plotted as a heatmap and clustered into three groups (Cluster A to C) (Figure 4, and Supplementary Table S4). We found 22 ASVs (30.1%) in Cluster A, which were more prevalent among the early responders while 12 of them were significantly different between response groups with an increased relative abundance along with treatment course. Among the significant ASVs, 4 were members of genus *Burkholderia* (gBurkh.39c8, gBurkh.6364, gBurkh.f802, and gBurkh.ee2f), 2 were genus *Acinetobacter* (gAcine.efe8, and gAcine.32b4), and the rest were members of genus *Corynebacterium* (gCoryn.ca4d), *Streptococcus* (gStrep.3ed3), *Brevundimonas* (gBrevu.1285), *Enhydrobacter* (gEnhyd.0ef3), *Candidatus Rhodoluna* (gCandi.9a10), and unspecified order Bacillales (oBacil.0094). In Cluster B (n=37), most of the ASVs had relatively small difference between response groups and were found no statistically significant difference across treatment. Four ASVs showing significant difference across treatment (assigned to genus *Corynebacterium* (gCoryn.1650, gCoryn.5ba9), unclassified family Methylobacteriaceae (fMethy.ebba), and unclassified family

Bradyrhizobiaceae (fBrady.cbae)). For Cluster C, 14 ASVs were more among the late responders compared to the early responders with dynamic trajectories (increased, decreased, and relatively stable in differece) over treatment. Twelve of them found statistically significant which were the members of genus *Acinetobacter* (gAcine.4f58, gAcine.4c95, and gAcine.dfae), genus *Thermus* (gTherm.b26c, gTherm.94db, and gTherm.087b), genus *Ralstonia* (gRalst.edc7 and gRalst.a529), genus *Corynebacterium* (gCoryn.ff32, gCoryn.0838), genus *Staphylococcus* (gStaph.ab0b), and unspecified family Caulobacteraceae (fCaulo.a200).

Discussion

In the present study, we have addressed temporal changes of the commensal microbiome in response to radiotherapy-based anticancer treatment among NPC patients for the first time. To be specific, the temporal changes in between-sample diversity of the nasopharyngeal microbiome and the abundant microbial features are associated with NPC patients' clinical responses. The longitudinal study design provided a comprehensive view of microbial diversity, an effective way for assessing the microbial correlation networks and an opportunity to reveal the degree of change of the abundant features between time points during the observation period (11). Notably, the subject-specific changes showed in our study might suggest a possibility of using the nasopharyngeal microbiome as a predictor for clinical response.

We observed that the UniFrac distances used for measuring beta-diversity qualitatively (unweighted) and quantitatively (weighted), on average, showed temporal changes throughout treatment (volatilities along PC1 explaining the largest amount of within-subject changes). Previous studies also described the progressive alteration in the oral microbiome during

radiotherapy among NPC patients (12), and the change in gut microbiome in patients after pelvic radiotherapy (13). Remarkably, we found distinct and consistent separations in volatility regarding patients' clinical responses along the PC2, which suggests that a global difference between the early and late responders might have existed before treatment and stay relatively stable afterward until the completion of radiotherapy. We further demonstrated that the magnitude of longitudinal global changes of the nasopharyngeal microbiome was significantly different between response groups, namely the average step length of the early responders was statistically, significantly larger than that of the late responders. However, the magnitude of changes appeared constant within each group along with treatment. These findings challenge the Anna Karenina principle, which suggests the positive prognosis is associated with community stability (14). It may implicate bacterial resilience to radiotherapy as a feature of delayed response. It is reasonable to imagine that such a community might be protective in some way against both radiation-induced perturbations on the microbiome as well as the host.

In the feature-based analysis, we observed similar characteristics in the NMIT analysis: the temporal changes in microbial networks of NPC patients over treatment were statistically significantly different regarding their clinical responses. The difference observed between groups was not due to a large degree of dispersion within groups. By looking at individual abundant ASV, genera known to dominate the human upper aerodigestive tract: *Corynebacterium*, *Staphylococcus*, *Acinetobacter*, and *Streptococcus* (15, 16), were also found dominant in our study. We found a significant and consistent loss of *Corynebacterium* (including 7 distinct ASVs) over treatment. Oral *Corynebacterium* was reported previously to decrease the risk of head and neck cancer, although the study did not include NPC (17). Members of the genera are also normally, temporally stable in Chinese adults (18).

Additionally, we observed that 28 out of 73 abundance ASVs were significantly different in abundance between the early and late responders during treatment. Notably, 10 ASVs primarily found in Cluster C differed between groups before the initiation of radiotherapy-based treatment and consistently differed until the completion. These results correspond to the characteristics observed in the diversity-based analyses above. Moreover, genera *Ralstonia* and *Thermus* have been previously identified as reagent contaminants (19). We found consistent signals for 4 ASVs from these genera (Ther-b26c, Ther-087b, Rals-edc7, and Rals-a529) between response groups, despite sample randomization across plates. These organisms were at very low abundance or absent in early responders, but present in late responders. Thus, the finding is unlikely solely due to contamination. Members of these extremophile genera are known to be radiation- or ROS-resistant, which suggests a potentially plausible biological mechanism for their inclusion in these communities (20). These findings suggest a possibility that these ASVs might be putative indicators of patients' response to radiotherapy-based treatment. . However, it is also important to note that some ASVs assigned to the same genus behaved differently, such as members of the genus *Acinetobacter* (gAcine.32b4 and gAcine.efe8 in Cluster A, compared to gAcine.4f58, gAcine.4c95, and gAcine.dfae in Cluster C), which may reflect niche specialization within the same genus (11).

While the results suggest a clear relationship between changes in the microbiome and treatment response, several open questions remain. First, previous studies in the literature focused mainly on potential associations between the commensal microbiome and the radiotherapy-induced side effects and comorbidities among cancer patients (12, 21-24), and rarely investigated the impact of microbiome on radiotherapy efficacy except a pilot study with a small sample size (n=3) which reported a relationship between the response to radiotherapy and the gut microbiome in pediatric cancer patients (25). It is, however, difficult

to compare our findings directly with most of the published data. Replication studies will be needed to determine if the microbiome can be used as a reliable indicator of treatment response in NPC. In addition, we acknowledge that the majority of our study subjects were NPC patients with stage III to IVb diseases (more than 90%) who were administrated concurrent chemo-radiotherapy (platinum-based) as recommended by clinical guidelines, and the analyses were not adjusted by therapeutic strategies due to a concern of low statistical power. The response to platinum-based chemotherapy has been reported to be modulated by gut microbiota, which influences the inflammation, immunity, and metabolism systematically (2, 26). Our analyses could not distinguish the contributions from radiotherapy and chemotherapy, separately. However, we considered that the nasopharyngeal microbiome might be affected mainly and heavily by radiotherapy with high energy X-ray in the nasopharynx. Last but not the least, some researchers suggest that microbiome affects the response to radiotherapy by modulating the damage-associated molecular pattern signals, however, the essential knowledge is yet deficient and the underlying mechanism is yet to be explored (2, 4, 27). Therefore, additional work is warranted to replicate our findings among similar study populations; and to address potential mechanisms, such as immune regulation and potential interaction between the nasopharyngeal microbiome and systemic immunotherapy.

In conclusion, this study demonstrated the temporal changes of the nasopharyngeal microbiome in NPC patients during radiotherapy-based treatment and suggested a significant association with clinical response. By focusing on NPC, a type of cancer where radiotherapy is the most common treatment, we hypothesize that the relationship between the microbiome and clinical response may hold true for other diseases and anatomical locations. These results shed new light on a possibility that the commensal microbiome may influence the response to

radiotherapy-based anticancer treatment in cancer patients, and call for larger longitudinal studies with long-term follow-up to understand the underlying mechanisms.

Materials and Methods

Study design and setting

This prospective study recruited newly diagnosed NPC patients in the First Affiliated Hospital of Guangxi Medical University, Guangxi Province located in southern China, between 2014 and 2015. The study was approved by the Ethical Review Committee of the First Affiliated Hospital of Guangxi Medical University, China, and the Regional Ethical Review Board in Stockholm, Sweden. Written informed consent was obtained from all patients. A total of 76 NPC patients were recruited and 62 were enrolled in this study. Details are given in Supplementary Data (Supplementary Method S1 and Figure S4).

All patients were treated according to the standards of clinical practice (details are given in Supplementary Method S2). All patients received the first clinical check-up at 3 months after the completion of radiotherapy and were followed up for 24 months. Patients who achieved a complete response (CR) in the first check-up were classified as early responders and patients who achieved CR between the first and the end of follow-up were designated late responders.

Sample collection and processing

In total 870 nasopharyngeal swabs were collected from 62 NPC patients. A protocol including enzymatic lysis and bead beating for DNA extraction was used. The indexed library

297 targeting the V3-V4 hypervariable regions of the 16S rRNA gene was prepared using samples
298 with sufficiently high-quality DNA. Extraction controls, PCR amplification controls, and
299 bacterial reference controls were included in each step. After quality and quantity checking, a
300 total of 526 16S rRNA-based libraries and 85 control libraries were sequenced by Beijing
301 Genomics Institute (BGI, Wuhan, China), using a 300-bp paired-end strategy on Illumina
302 Miseq according to the manufacturer's instructions. Details are given in Supplementary Data
303 (Supplementary Method S3 and S4, and Figure S4).

304

305 *Data denoising and pre-processing*

306 Raw sequences were quality filtered and denoised using *deblur* to generated amplicon
307 sequence variants (ASVs) in QIIME 2 (v. 2019-10) (28-31). A phylogenetic tree was built
308 using fragment insertion into the August 2013 Greengenes 99% tree and taxonomic
309 assignments using a naïve Bayesian classifier trained against the same reference (32-34). The
310 dataset was filtered to remove samples without valid clinical information (4 individuals with
311 56 samples), ASVs assigned to mitochondrial rRNA (35), and samples with fewer than 1,500
312 reads (25 samples). Finally, 445 samples derived from 39 NPC patients were retained, with
313 around 3 million high quality reads assigned to 9,320 ASVs (33 phyla, 107 classes, 192 orders,
314 336 families, and 724 genera). Between-sample diversity (beta-diversity) was estimated after
315 samples were rarefied to 1,500 reads per sample (36). Feature-based analyses were performed
316 using a representative subset of ASVs with at least 0.1% relative abundance in at least 10% of
317 samples, as abundant ASVs (n=73). Two samples were removed due to the absence of
318 abundant ASVs, retaining 443 samples. The concordance between the main ASVs dataset and
319 the abundant ASVs subset was tested. Details are given in Supplementary Data
320 (Supplementary Method S5 and Figure S5).

321

322 *Statistical analysis*

323 In this study, the analyses of global patterns were mainly focused on beta-diversity using
324 unweighted and weighted UniFrac distance (37, 38). Principal Coordinate Analysis (PCoA)
325 projections were used to visualize between-sample difference (39). The longitudinal pattern of
326 nasopharyngeal microbiome along each principle coordinate (PC) was visualized using
327 volatility analysis in QIIME 2 2019.10 (*q2-longitudinal*) (40). The weighted UniFrac distance
328 matric was further used to measure the rate of change which differed over treatment. The
329 change in an individual community between two sequential treatment occasions was
330 quantified as the weighted UniFrac distance between successive samples (Δ-wUF = $wUF_{(t)}$ –
331 $wUF_{(t-1)}$), corresponding to the weighted Unifrac step length of an individual's trajectory
332 through nasopharyngeal microbial space. Δ-wUF was modeled as a function of treatment
333 occasion (sampling time) via linear mixed effect models (LMEs, considering treatment,
334 temporal and inter-individual effects) with the *lme4* package (v. 1.1-19) in R 3.5.1 (41).
335 Differences between nested models were tested via likelihood ratio tests, while Akaike's
336 information criterion (AIC) was used to compare general models.

337

338 In the analyses of feature-based patterns, Non-parametric Microbial Interdependence Test
339 (NMIT) was used to determine longitudinal sample similarity as a function of temporal
340 microbial composition network over treatment (42). We further eliminated three patients who
341 had less than five successive samples, retaining 434 samples of 36 patients, to make the
342 analysis robust and efficient. In brief, the Spearman correlations between any pair of 73
343 abundant ASVs were computed based on their relative abundance; distances between any two
344 of patients' correlation matrices were calculated based on a Frobenius norm; PCoA was used

to visualize the similarity among patients. The difference of microbial networks between response groups was tested by the permutation-based extension of multivariate analysis of variance (PERMANOVA) test (43) and the multivariate dispersion test (permdisp) (44). NMIT, PERMANOVA, and permdisp were carried out by QIIME 2 2019.10, and PCoA was plotted in R 3.5.1. On the other hand, the longitudinal patterns of the 73 abundant ASVs individually were also analyzed. The temporal relationship for the abundant ASVs was evaluated using a modified analysis of composition of microbiomes (ANCOM)-based approach using Spearman correlation (45). A normalized ANCOM W statistic was calculated as the fraction of tests where the raw p-values were less than 0.05, and a normalized W of more than 80% was considered statistically significant. This test was applied to both the raw data, and the ratios between time points. Additionally, the longitudinal differences in abundance (log2-transformed) of abundant ASVs between early and late responders were modeled via Smoothing-spline ANOVA (SS-ANOVA) (46) using *metagenomeSeq* package (v. 1.24.0); the predicted changing trajectories of abundant ASVs were grouped into hierarchical clustering using Ward's method (Ward's D2) and displayed as a heatmap using *Heatplus* package (v. 2.32.1) (47) in R.3.6.2.

Data availability

Raw sequencing data and metadata are deposited in ENA under accession XXXXX.

Acknowledgements

We acknowledge funding from the Swedish Cancer Society (2016/510 to W. Ye) and the Swedish Research Council (2015-02625, 2015-06268, 2017-05814 to W. Ye); the National Natural Science Foundation of China (81360405 to R. Wang) and the Guangxi (China) Science and Technology Program Project (GK AD17129013 to R. Wang); the Natural Science Foundation of Guangxi Medical University for Junior Scientists (GXMUYSF201203 to T. Huang). T. Huang was also partly supported by a grant from the China Scholarship Council (201408450018).

We would like to thank the patients recruited in this study, and the clinical staff in the Department of Radiation Oncology in the First Affiliated Hospital of Guangxi Medical University (Nanning, P. R. China). We are grateful to Dr. Zhe Zhang, Dr. Xiaoying Zhou, Dr. Xue Xiao, and their research group for lab support.

T. Huang had full access to all of the data in the study and takes responsibility for the integrity of the data and the accuracy of the data analysis. T. Huang, Z. Zhang, R. Wang, and W. Ye conceived and designed the study. T. Huang, R. Wang, and W. Ye received funding. T. Huang, T. Zhang, and K. Hu recruited patients, collected samples and follow-up information. T. Huang and X. Xiao performed laboratory assays. Z. Zhang, R. Wang, and W. Ye contributed resources. T. Huang, J. Debelius, and A. Ploner analyzed the data, prepared figures. T. Huang, J. Debelius, A. Ploner, R. Wang, and W. Ye interpreted the results. T. Huang, J. Debelius, and A. Ploner wrote the manuscript. All authors edited the manuscript and approval of the final draft.

On behalf of all authors, the corresponding authors declared that they have no potential financial and non-financial competing interests.

References

1. Garrett WS. 2015. Cancer and the microbiota. Science 348:80-6.

2. Roy S, Trinchieri G. 2017. Microbiota: a key orchestrator of cancer therapy. Nat Rev Cancer 17:271-285.

3. McQuade JL, Daniel CR, Helmink BA, Wargo JA. 2019. Modulating the microbiome to improve therapeutic response in cancer. Lancet Oncol 20:e77-e91.

4. Raza MH, Siraj S, Arshad A, Waheed U, Aldakheel F, Alduraywish S, Arshad M. 2017. ROS-modulated therapeutic approaches in cancer treatment. J Cancer Res Clin Oncol doi:10.1007/s00432-017-2464-9.

5. Geller LT, Barzily-Rokni M, Danino T, Jonas OH, Shental N, Nejman D, Gavert N, Zwang Y, Cooper ZA, Shee K, Thaiss CA, Reuben A, Livny J, Avraham R, Frederick DT, Ligorio M, Chatman K, Johnston SE, Mosher CM, Brandis A, Fuks G, Gurbatri C, Gopalakrishnan V, Kim M, Hurd MW, Katz M, Fleming J, Maitra A, Smith DA, Skalak M, Bu J, Michaud M, Trauger SA, Barshack I, Golan T, Sandbank J, Flaherty KT, Mandinova A, Garrett WS, Thayer SP, Ferrone CR, Huttenhower C, Bhatia SN, Gevers D, Wargo JA, Golub TR, Straussman R. 2017. Potential role of intratumor bacteria in mediating tumor resistance to the chemotherapeutic drug gemcitabine. Science 357:1156-1160.

6. Routy B, Le Chatelier E, Derosa L, Duong CPM, Alou MT, Daillere R, Fluckiger A, Messaoudene M, Rauber C, Roberti MP, Fidelle M, Flament C, Poirier-Colame V, Opolon P, Klein C, Iribarren K, Mondragon L, Jacquelot N, Qu B, Ferrere G, Clemenson C, Mezquita L, Masip JR, Naltet C, Brosseau S, Kaderbhai C, Richard C, Rizvi H, Levenez F, Galleron N, Quinquis B, Pons N, Ryffel B, Minard-Colin V, Gonin P, Soria JC, Deutsch E, Loriot Y, Ghiringhelli F, Zalcman G, Goldwasser F, Escudier B, Hellmann MD, Eggermont A, Raoult D, Albiges L, Kroemer G, Zitvogel L. 2018. Gut microbiome influences efficacy of PD-1-based immunotherapy against epithelial tumors. Science 359:91-97.

412 7. Helmink BA, Khan MAW, Hermann A, Gopalakrishnan V, Wargo JA. 2019. The microbiome,
413 cancer, and cancer therapy. Nat Med 25:377-388.
414 8. Chua MLK, Wee JTS, Hui EP, Chan ATC. 2016. Nasopharyngeal carcinoma. Lancet 387:1012-
415 1024.
416 9. Lee AW, Ma BB, Ng WT, Chan AT. 2015. Management of Nasopharyngeal Carcinoma: Current
417 Practice and Future Perspective. J Clin Oncol 33:3356-64.
418 10. Hong RL, Hsiao CF, Ting LL, Ko JY, Wang CW, Chang JTC, Lou PJ, Wang HM, Tsai MH, Lai SC, Liu
419 TW. 2018. Final results of a randomized phase III trial of induction chemotherapy followed by
420 concurrent chemoradiotherapy versus concurrent chemoradiotherapy alone in patients with
421 stage IVA and IVB nasopharyngeal carcinoma-Taiwan Cooperative Oncology Group (TCOG)
422 1303 Study. Ann Oncol 29:1972-1979.
423 11. Goodrich JK, Di Rienzi SC, Poole AC, Koren O, Walters WA, Caporaso JG, Knight R, Ley RE.
424 2014. Conducting a microbiome study. Cell 158:250-262.
425 12. Zhu XX, Yang XJ, Chao YL, Zheng HM, Sheng HF, Liu HY, He Y, Zhou HW. 2017. The Potential
426 Effect of Oral Microbiota in the Prediction of Mucositis During Radiotherapy for
427 Nasopharyngeal Carcinoma. Ebiomedicine 18:23-31.
428 13. Wang A, Ling Z, Yang Z, Kiela PR, Wang T, Wang C, Cao L, Geng F, Shen M, Ran X, Su Y, Cheng
429 T, Wang J. 2015. Gut microbial dysbiosis may predict diarrhea and fatigue in patients
430 undergoing pelvic cancer radiotherapy: a pilot study. PLoS One 10:e0126312.
431 14. Zaneveld JR, McMinds R, Vega Thurber R. 2017. Stress and stability: applying the Anna
432 Karenina principle to animal microbiomes. Nat Microbiol 2:17121.
433 15. Wang H, Dai W, Feng X, Zhou Q, Wang H, Yang Y, Li S, Zheng Y. 2018. Microbiota Composition
434 in Upper Respiratory Tracts of Healthy Children in Shenzhen, China, Differed with Respiratory
435 Sites and Ages. Biomed Res Int 2018:6515670.

16. Hang J, Zavaljevski N, Yang Y, Desai V, Ruck RC, Macareo LR, Jarman RG, Reifman J, Kuschner RA, Keiser PB. 2017. Composition and variation of respiratory microbiota in healthy military personnel. PLoS One 12:e0188461.

17. Hayes RB, Ahn J, Fan X, Peters BA, Ma Y, Yang L, Agalliu I, Burk RD, Ganly I, Purdue MP, Freedman ND, Gapstur SM, Pei Z. 2018. Association of Oral Microbiome With Risk for Incident Head and Neck Squamous Cell Cancer. JAMA Oncol 4:358-365.

18. Utter DR, Mark Welch JL, Borisy GG. 2016. Individuality, Stability, and Variability of the Plaque Microbiome. Front Microbiol 7:564.

19. Salter SJ, Cox MJ, Turek EM, Calus ST, Cookson WO, Moffatt MF, Turner P, Parkhill J, Loman NJ, Walker AW. 2014. Reagent and laboratory contamination can critically impact sequence-based microbiome analyses. BMC Biol 12:87.

20. Battista JR, Earl AM, Park MJ. 1999. Why is Deinococcus radiodurans so resistant to ionizing radiation? Trends Microbiol 7:362-5.

21. Reis Ferreira M, Andreyev HJN, Mohammed K, Truelove L, Gowan SM, Li J, Gulliford SL, Marchesi JR, Dearnaley DP. 2019. Microbiota- and Radiotherapy-Induced Gastrointestinal Side-Effects (MARS) Study: A Large Pilot Study of the Microbiome in Acute and Late-Radiation Enteropathy. Clin Cancer Res 25:6487-6500.

22. Hou J, Zheng H, Li P, Liu H, Zhou H, Yang X. 2018. Distinct shifts in the oral microbiota are associated with the progression and aggravation of mucositis during radiotherapy. Radiother Oncol doi:10.1016/j.radonc.2018.04.023.

23. Zhang J, Liu H, Liang X, Zhang M, Wang R, Peng G, Li J. 2015. Investigation of salivary function and oral microbiota of radiation caries-free people with nasopharyngeal carcinoma. PLoS One 10:e0123137.

24. Wang Z, Wang Q, Wang X, Zhu L, Chen J, Zhang B, Chen Y, Yuan Z. 2019. Gut microbial dysbiosis is associated with development and progression of radiation enteritis during pelvic radiotherapy. J Cell Mol Med 23:3747-3756.

462 25. Sahly N, Moustafa A, Zaghloul M, Salem TZ. 2019. Effect of radiotherapy on the gut
463 microbiome in pediatric cancer patients: a pilot study. PeerJ 7:e7683.
464 26. Iida N, Dzutsev A, Stewart CA, Smith L, Bouladoux N, Weingarten RA, Molina DA, Salcedo R,
465 Back T, Cramer S, Dai RM, Kiu H, Cardone M, Naik S, Patri AK, Wang E, Marincola FM, Frank
466 KM, Belkaid Y, Trinchieri G, Goldszmid RS. 2013. Commensal bacteria control cancer response
467 to therapy by modulating the tumor microenvironment. Science 342:967-70.
468 27. Al-Qadami G, Van Sebille Y, Le H, Bowen J. 2019. Gut microbiota: implications for
469 radiotherapy response and radiotherapy-induced mucositis. Expert Rev Gastroenterol
470 Hepatol 13:485-496.
471 28. Bolyen E, Rideout JR, Dillon MR, Bokulich NA, Abnet CC, Al-Ghalith GA, Alexander H, Alm EJ,
472 Arumugam M, Asnicar F, Bai Y, Bisanz JE, Bittinger K, Brejnrod A, Brislawn CJ, Brown CT,
473 Callahan BJ, Caraballo-Rodriguez AM, Chase J, Cope EK, Da Silva R, Diener C, Dorrestein PC,
474 Douglas GM, Durall DM, Duvallet C, Edwardson CF, Ernst M, Estaki M, Fouquier J, Gauglitz JM,
475 Gibbons SM, Gibson DL, Gonzalez A, Gorlick K, Guo J, Hillmann B, Holmes S, Holste H,
476 Huttenhower C, Huttley GA, Janssen S, Jarmusch AK, Jiang L, Kaehler BD, Kang KB, Keefe CR,
477 Keim P, Kelley ST, Knights D, et al. 2019. Reproducible, interactive, scalable and extensible
478 microbiome data science using QIIME 2. Nat Biotechnol 37:852-857.
479 29. Bokulich NA, Kaehler BD, Rideout JR, Dillon M, Bolyen E, Knight R, Huttley GA, Gregory
480 Caporaso J. 2018. Optimizing taxonomic classification of marker-gene amplicon sequences
481 with QIIME 2's q2-feature-classifier plugin. Microbiome 6:90.
482 30. Amir A, McDonald D, Navas-Molina JA, Kopylova E, Morton JT, Zech Xu Z, Kightley EP,
483 Thompson LR, Hyde ER, Gonzalez A, Knight R. 2017. Deblur Rapidly Resolves Single-
484 Nucleotide Community Sequence Patterns. mSystems 2.
485 31. Bokulich NA, Subramanian S, Faith JJ, Gevers D, Gordon JI, Knight R, Mills DA, Caporaso JG.
486 2013. Quality-filtering vastly improves diversity estimates from Illumina amplicon sequencing.
487 Nat Methods 10:57-9.

488 32. McDonald D, Price MN, Goodrich J, Nawrocki EP, DeSantis TZ, Probst A, Andersen GL, Knight
489 R, Hugenholtz P. 2012. An improved Greengenes taxonomy with explicit ranks for ecological
490 and evolutionary analyses of bacteria and archaea. ISME J 6:610-8.
491 33. Wang Q, Garrity GM, Tiedje JM, Cole JR. 2007. Naive Bayesian classifier for rapid assignment
492 of rRNA sequences into the new bacterial taxonomy. Appl Environ Microbiol 73:5261-7.
493 34. Janssen S, McDonald D, Gonzalez A, Navas-Molina JA, Jiang L, Xu ZZ, Winker K, Kado DM,
494 Orwoll E, Manary M, Mirarab S, Knight R. 2018. Phylogenetic Placement of Exact Amplicon
495 Sequences Improves Associations with Clinical Information. mSystems 3.
496 35. Emelyanov VV. 2001. Evolutionary relationship of Rickettsiae and mitochondria. FEBS Lett
497 501:11-8.
498 36. Weiss S, Xu ZZ, Peddada S, Amir A, Bittinger K, Gonzalez A, Lozupone C, Zaneveld JR,
499 Vazquez-Baeza Y, Birmingham A, Hyde ER, Knight R. 2017. Normalization and microbial
500 differential abundance strategies depend upon data characteristics. Microbiome 5:27.
501 37. Lozupone CA, Hamady M, Kelley ST, Knight R. 2007. Quantitative and qualitative beta
502 diversity measures lead to different insights into factors that structure microbial
503 communities. Appl Environ Microbiol 73:1576-85.
504 38. Lozupone C, Knight R. 2005. UniFrac: a new phylogenetic method for comparing microbial
505 communities. Appl Environ Microbiol 71:8228-35.
506 39. Vazquez-Baeza Y, Pirrung M, Gonzalez A, Knight R. 2013. EMPeror: a tool for visualizing high-
507 throughput microbial community data. Gigascience 2:16.
508 40. Bokulich NA, Dillon MR, Zhang Y, Rideout JR, Bolyen E, Li H, Albert PS, Caporaso JG. 2018. q2-
509 longitudinal: Longitudinal and Paired-Sample Analyses of Microbiome Data. mSystems 3.
510 41. Bates D, Mächler M, Bolker B, Walker S. 2015. Fitting Linear Mixed-Effects Models Using
511 lme4. 2015 67:48.

512 42. Zhang Y, Han SW, Cox LM, Li H. 2017. A multivariate distance-based analytic framework for
513 microbial interdependence association test in longitudinal study. Genet Epidemiol 41:769-
514 778.
515 43. Anonymous. Permutational Multivariate Analysis of Variance (PERMANOVA), p 1-15, Wiley
516 StatsRef: Statistics Reference Online doi:10.1002/9781118445112.stat07841.
517 44. Anderson MJ, Ellingsen KE, McArdle BH. 2006. Multivariate dispersion as a measure of beta
518 diversity. Ecol Lett 9:683-93.
519 45. Mandal S, Van Treuren W, White RA, Eggesbo M, Knight R, Peddada SD. 2015. Analysis of
520 composition of microbiomes: a novel method for studying microbial composition. Microb
521 Ecol Health Dis 26:27663.
522 46. Joseph N. Paulson HT, Hector Corrada Bravo. 2017. Longitudinal differential abundance
523 analysis of microbial marker-gene surveys using smoothing splines. bioRxiv
524 doi:https://doi.org/10.1101/099457.
525 47. Ploner A. 2018. Heatplus: Heatmaps with row and/or column covariates and colored clusters.
526 https://github.com/alexploner/Heatplus,

527

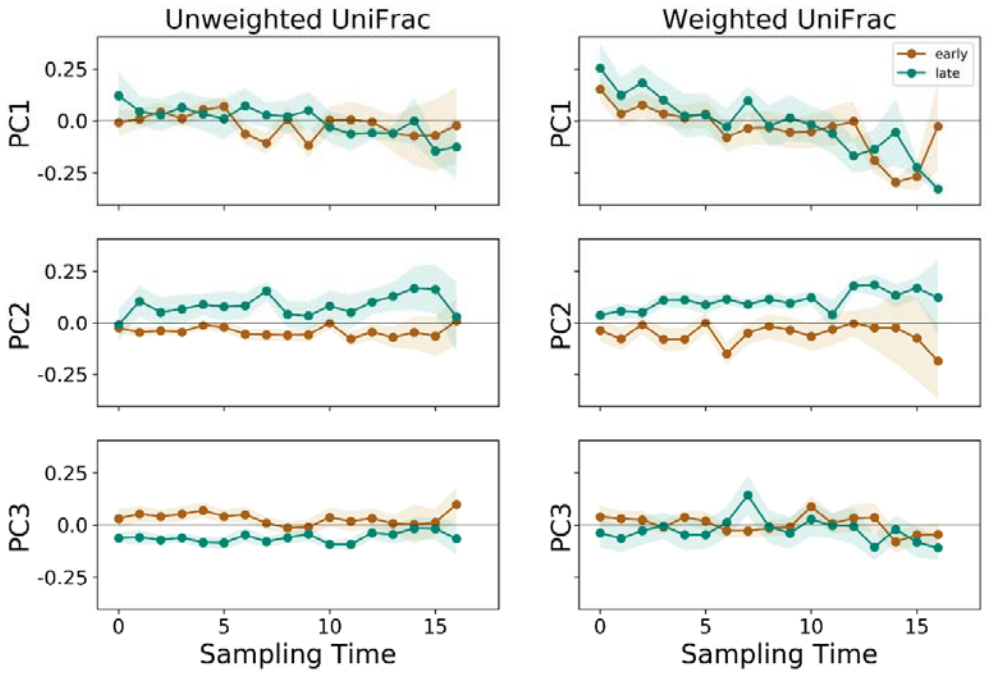

528

529 **Figure 1. Normalized volatility of the nasopharyngeal microbiome in 39 patients during**
530 **a 7-week treatment course.**

531 The longitudinal pattern of the nasopharyngeal microbiome of 39 patients over 7-week
532 treatment was explored by Principle Coordinate Analysis (PCoA) projection along principle
533 coordinate1 (PC1), PC2 and PC3 with regard to sampling time. The volatility analysis was
534 used to visualize the mean distances based on UniFrac distance matrices in each PC space.
535 The left of each panel reflects mean volatility of all individual trajectories referred to the
536 unweighted UniFrac distance matrix, and the right side referred to the weighted UniFrac
537 distance matrix. The consecutive numbers on the bottom indicate the sampling time points (0
538 = before radiotherapy). The trace represents the mean and the shaded is the standard deviation
539 of each sampling time point. The curves in each PC space are marked by response status (a
540 brown curve showing the early responders, a green curve showing the late responders).

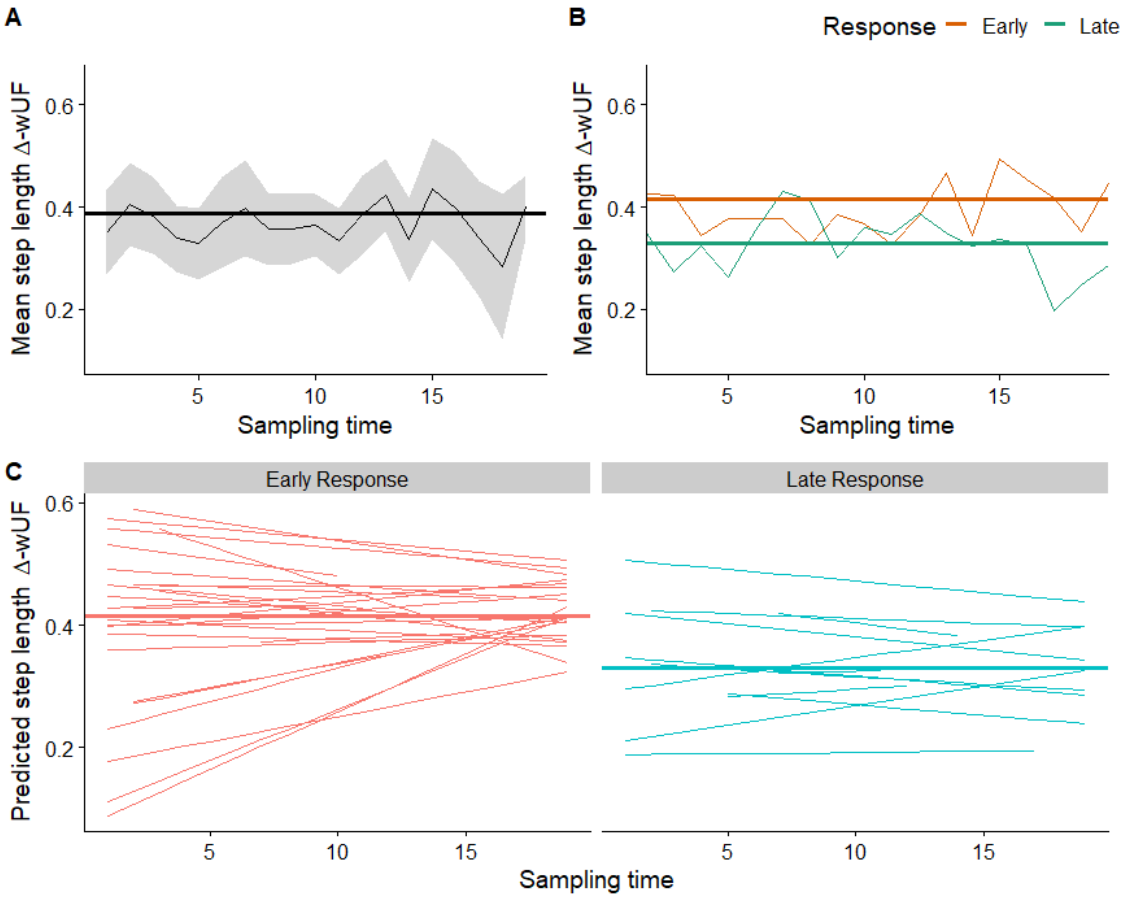

Figure 2. Group-wise and individual Δ-wUFs during treatment reflect the rate of change in the community.

The weighted UniFrac step length Δ-wUF of an individual's trajectory through nasopharyngeal microbial space was modeled as a function of treatment occasion (sampling time) via linear mixed effect models (LMEs), including within-individual random effects. The consecutive numbers on the bottom of each panel indicate the sampling time points. We explored (Panel A) the average step length across all individuals and (Panel B) average step length by clinical response. The moving average is shown as a thin line with shaded pointwise 95% confidence intervals; the thicker line is the estimated average step length (fixed effect) from the mixed model which takes into account the individual-level variations in step length over sampling time. We also explored the predicted individual step length trajectories for

553 early and late responders (Panel C). The horizontal axis indicates the sampling time during

554 treatment and the vertical axis the mean step length Δ-wUFs.

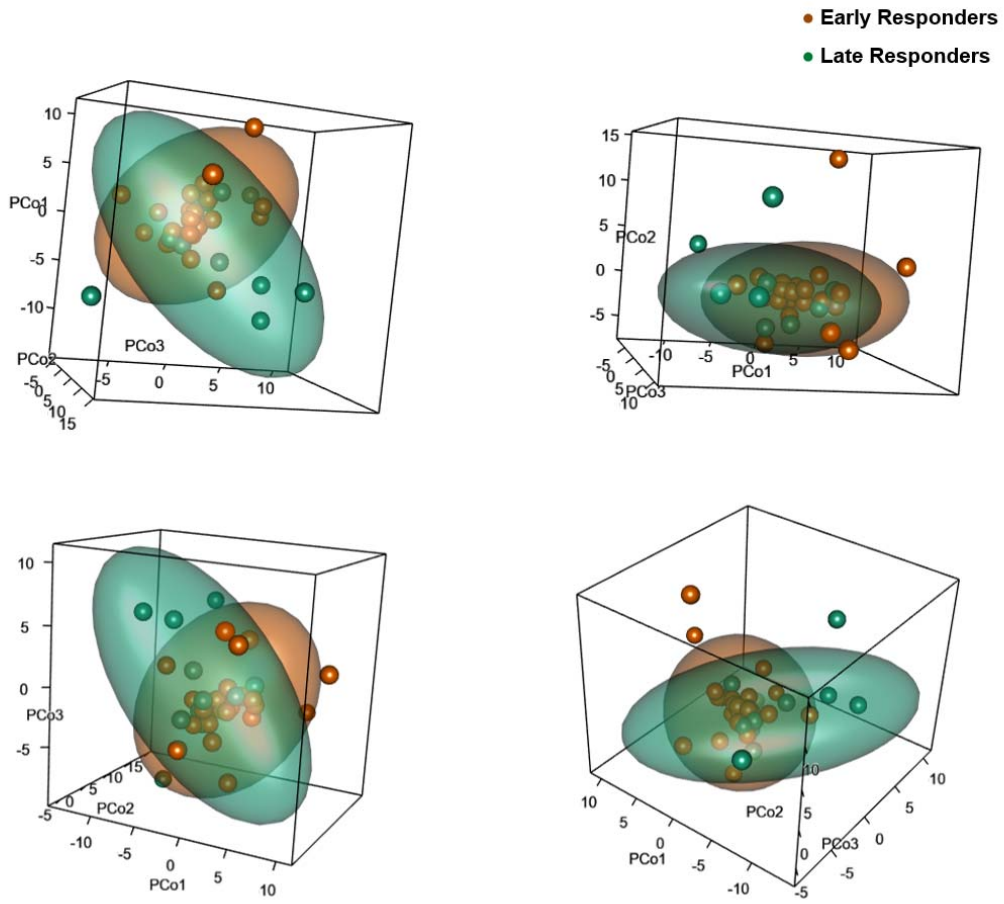

Figure 3. Differences in the interdependence networks of nasopharyngeal microbiome between the early and late responders.

Non-parametric microbial interdependence test (NMIT) was used to determine longitudinal sample similarity as a function of temporal microbial composition networks over treatment. The similarities of nasopharyngeal microbial networks among NPC patients were visualized by Principle Coordinate Analysis (PCoA) projection. The first 3 axes in PCoA explain 15.03% of the variation in total (PCo1=5.67%, PCo2=4.91%, PCo3=4.45%). Each dot in the PCoA space is an indicator representing the temporal microbial network of one NPC patient. Brown dots are the early responders, green the late responders. The cloud representing the minimum-volume ellipsoid covers 80% of the data of each group. Panels A-D reflect different orientations of the same 3-dimention plot (screenshots from a 3-dimension PCoA projection).

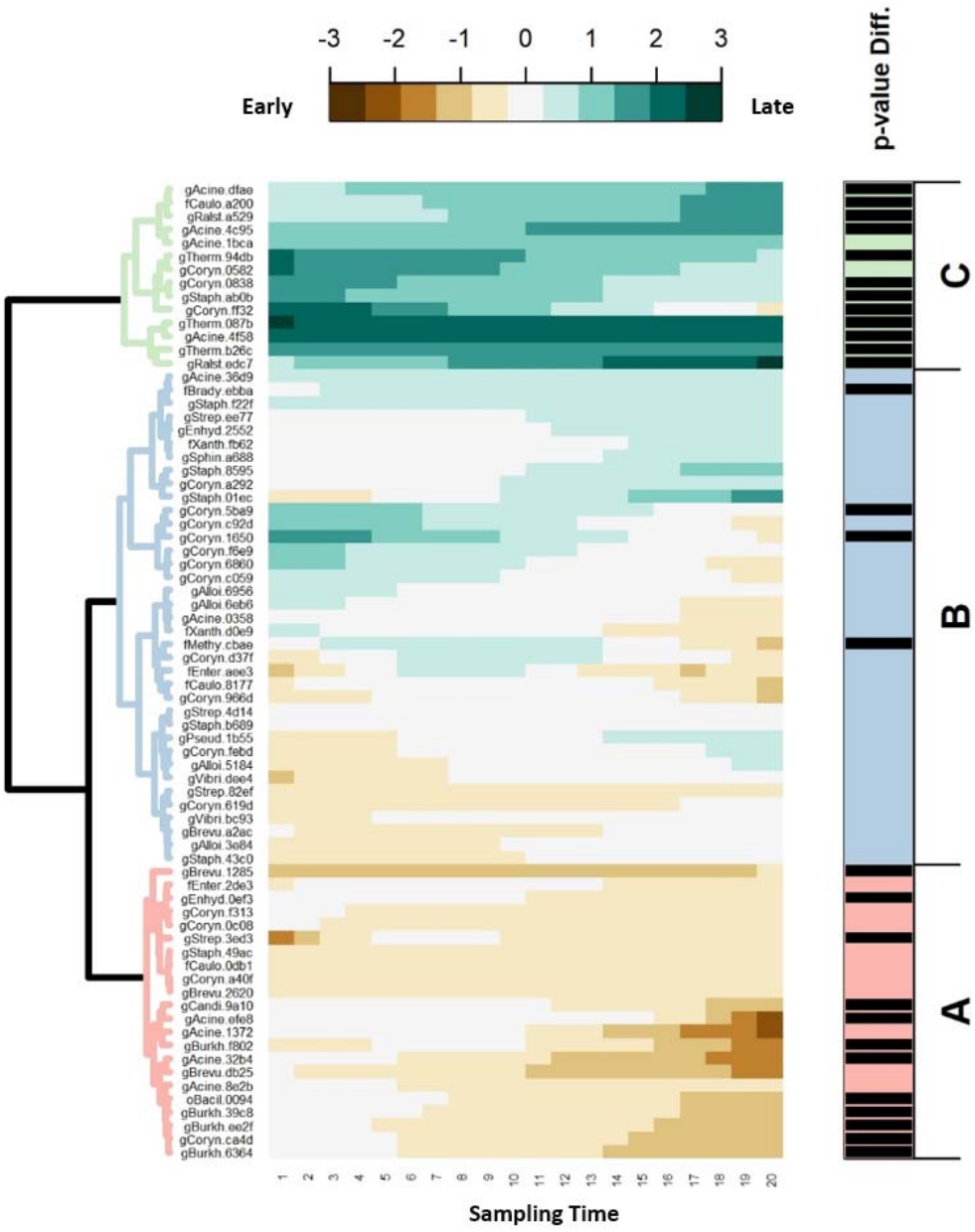

567

568 **Figure 4. The predicted log2-fold change trajectories of 73 abundant ASVs between the**

569 **early and late responders.**

The predicted log2-fold change trajectories of 73 amplicon sequence variants (ASVs) between the early responders and late responders generated from SS-ANOVA were grouped into hierarchical clusters using Ward's D2 and displayed as a heatmap. Each raw in the heatmap represents the trajectory across treatment of each ASV. The consecutive numbers on the bottom of heatmap indicate the sampling time points (1 = before radiotherapy, 20 = end of radiotherapy). ASVs with higher abundance in early responders are brown; those with more abundance in late responders are teal. Three clusters are marked as A to C. The vertical bars on the right side indicate whether the trend in difference across treatment is statistically significant (*P*-value < 0.05 for the black bars, otherwise not).

579 **Table 1. Twenty-eight abundant ASVs were detected with significant differences**

580 **between early and late responders during a 7-week treatment course.**

		Time intervals[b]		Permutative[c]
ASV-ID	Taxonomy[a]	Start	End	*P*-value
gBurkh.6364	g__Burkholderia	7	20	0.005
gBurkh.39c8	g__Burkholderia	8	20	0.007
gCandi.9a10	g__Candidatus Rhodoluna	14	20	0.009
oBacil.0094	o__Bacillales	8	20	0.011
gAcine.32b4	g__Acinetobacter	7	20	0.011
gAcine.efe8	g__Acinetobacter	18	20	0.011
gEnhyd.0ef3	g__Enhydrobacter	10	20	0.018
gStrep.3ed3	g__Streptococcus	1	17	0.020
gBrevu.1285	g__Brevundimonas	1	19	0.024
gCoryn.ca4d	g__Corynebacterium	8	20	0.029
gBurkh.f802	g__Burkholderia	14	20	0.044
gBurkh.ee2f	g__Burkholderia	7	20	0.049
fMethy.cbae	f__Methylobacteriaceae	5	11	0.017
gCoryn.1650	g__Corynebacterium	1	12	0.026
fBrady.ebba	f__Bradyrhizobiaceae	6	20	0.029
gCoryn.5ba9	g__Corynebacterium	1	13	0.043
gTherm.b26c	g__Thermus	1	20	0.003
fCaulo.a200	f__Caulobacteraceae	2	20	0.003
gTherm.94db	g__Thermus	1	19	0.003
gTherm.087b	g__Thermus	1	20	0.004
gAcine.4f58	g__Acinetobacter	1	20	0.005
gRalst.edc7	g__Ralstonia	1	20	0.006
gAcine.4c95	g__Acinetobacter	1	20	0.009
gAcine.dfae	g__Acinetobacter	1	20	0.013
gCoryn.ff32	g__Corynebacterium	1	12	0.016
gStaph.ab0b	g__Staphylococcus	1	14	0.021
gCoryn.0838	g__Corynebacterium	1	15	0.025
gRalst.a529	g__Ralstonia	4	20	0.041

581 [a]: Taxonomy assignment. “g__” refers to genus; “f__” refers to family; “o__” refers to order.

582 [b]: Time intervals with significant difference; number refers to sampling time (1 = before radiotherapy,

583 20 = end of radiotherapy).

584 [c]: 1500 permutations.